Influence of ion pairing in ionic liquids on electrical double layer structures and surface force using classical density functional approach.

Ma, Ke; Forsman, Jan; Woodward, Clifford E

Published in:
Journal of Chemical Physics

DOI:
10.1063/1.4919314

2015

Influence of Ion Pairing in Ionic Liquids on Electrical Double Layer Structures and Surface Force Using Classical Density Functional Approach

Ke Ma and Clifford E. Woodward*

School of Physical,

Environmental and Mathematical Sciences

University of New South Wales,

Canberra at the Australian Defence Force Academy

Canberra ACT 2600, Australia

Jan Forsman

Theoretical Chemistry,

Chemical Centre, Lund University

P.O.Box 124, S-221 00 Lund, Sweden

Abstract

We explore the influence of ion pairing in room temperature ionic liquids confined by planar electrode surfaces. Using a coarse-grained model for the aromatic ionic liquid $[C_4MIM^+][BF_4^-]$, we account for an ion paring component as an equilibrium associating species within a classical density functional theory. We investigated the resulting structure of the electrical double layer as well as the ensuing surface forces and differential capacitance, as a function of the degree of ion association. We found that the short-range structure adjacent to surfaces was remarkably unaffected by the degree of ion pairing, up to several molecular diameters. This was even the case for 100% of ions being paired. The physical implications of ion pairing only become apparent in equilibrium properties that depend upon the long-range screening of charges, such as the asymptotic behaviour of surface forces and the differential capacitance, especially at low surface potential. The effect of ion pairing on capacitance is consistent with their invocation as a source of the anomalous temperature dependence of the latter. This work shows that ion pairing effects on equilibrium properties are subtle, and will not easily be observed in computer simulations.

*Electronic address: c.woodward@adfa.edu.au

I. INTRODUCTION

Ionic liquids have been intensively studied due to their great potential for applications in synthesis, catalysis and electric capacitors.[1–3] Room-temperature ionic liquids (RTILs) possess a variety of unique properties, which can be attributed to their chemical structure and combinations of anions and cations [4–6]. In contrast to typical inorganic electrolytes, the chemical structure of RTILs leads to a high electrochemical stability and asymmetric molecular shapes, essential for them to maintain a fluid phase [6, 7]. Furthermore, the strong electrostatic coupling in RTILs imparts a low vapour pressure, which makes them sought after as so-called "green solvents". When RTILs are in confined geometries, solid-like properties are observed at interfaces [8, 9]. Indeed, the strength of the electrostatic interactions suggests that RTILs are on the verge of crystallizing, but this is seemingly frustrated by steric effects.

The strength of electrostatic correlations in RTILs and their proximity to solidification has motivated the idea that they may be considered as a fluid where clusters of ions (Bjerrum clusters) are in equilibrium with free ions [10]. This is often articulated in terms of ion pair formation (between anions and cations), where pairs are the smallest in the hierarchy of possible ionic clusters. For example, recent surface force measurements of imidazolium-based RTILs by Gebbie *et al.* suggest a substantial fraction of ion pairs in equilibrium with free ionic species [11]. Using DLVO theory to fit the force-distance curves between gold and mica surfaces, immersed in an RTIL, those authors suggest a high degree of ion pairing is required to explain the long-range exponential decay of the forces. That is, the strong correlations between anions and cations which is manifested in cluster formation diminishes the ability of the RTIL to exhibit non-electroneutral fluctuations and thus compromises the screening of electrode charges. Cluster theories are well-known vehicles with which to describe strong correlations in electrolytes [10, 12]. However, the existence of significant numbers of ion pairs or clusters in RTILs remains a controversial topic [8].

This notwithstanding, ionic clusters have also been used to rationalize the unusual temperature dependence of the differential capacitance (DC) in electrical double layer(EDL) capacitors containing certain RTILs. However, it should be noted that contradictory results are found in both experimental and theoretical capacitance studies [6]. Drushchler *et al.* [13] applied different experimental techniques to analyse the temperature dependence of

broadband capacitance spectra with RTILs. Among the different time scales of interfacial dynamics, an overall decrease with temperature is observed for the fast capacitive process near gold electrodes, from 303K to 363K. On the other hand, Lockett *et al.* measured an increase of the DC from 295K to 333K in imidazolium based RTILs [14]. Costa *et al.* observed a positive temperature effect on the DC for both imidazolium and pyrrolidinium RTILs at Hg electrode.[15] and Alam *et al* [16] found that the temperature dependence of the DC for $[BMIM^+][BF_4^-]$ is positive (increases with temperature) at glassy carbon and gold electrodes but negative (decreases with temperature) at Hg electrodes. In a subsequent work, those authors found that around the potential of zero charge (PZC), the temperature dependence of the DC was negative for $[EMIM^+][BF_4^-]$ but positive for $[OMIM^+][BF_4^-]$ [9]. As suggested by a number of authors [15, 17–19], a positive temperature dependence of the DC can be explained by an increase in free charges, which is consistent with the existence of equilibrium ion clusters. The breakdown of such clusters at the electrified interface, as the temperature increases, leads to more ions being available for screening and a larger DC.

Recent Molecular Dynamics (MD) simulations by Vatamanu *et al.* predict a positive dependence of the DC with temperature at low potential at corrugated surfaces [20]. MD simulations by Liu *et al.* reported an increase in the DC in imidazolium based RTILs only, from 450K to 500K near positive electrodes [21]. This arose from the specific adsorption of the imidazolium ring at the electrode. An ion pairing mechanism has been applied in theories for molten inorganic salts, which have some common features with RTILs [22, 23]. An associated mean spherical approximation has been proposed to explain the effect of temperature on capacitance in these systems [24]. MC simulations of ion-dipole mixtures also indicate that the presence of ion pairs induces a strongly layered structure at both charged and neutral surface [22].

Tokuda *et al.* [25] discuss ion association in a dynamic setting through the concept of *ionicity*, which can be determined as a ratio of the measured conductivity and that predicted by the simple Nernst-Einstein relation. A value less than unity is then indicative of ion pair formation. A value of around 50%-70% pairing is not unusual for a variety of RTILs. The physical implications of ionic clusters in dynamic and equilibrium contexts is not straightforward. For example, to assert that neutral clusters do not contribute to conductivity is probably overstating their non-participation. That is, it is possible that ions will dissociate from one cluster and join another as a dynamic response to an electric field

over small time-scales [25]. This will raise the conductivity beyond what would normally be expected for a mixture of single ions and neutral clusters. Thus ion paring *per se* may more properly be seen as a manifestation of strong correlations, which slow diffusion over an intermediate time scale, rather than as very long-lived entities. In this context, Harris *et al.* have pointed out that an ionicity value less than unity can be attributed to correlations in ion velocities [26, 27].

In recent work, we have developed an accurate classical density functional theory (DFT) for generic coarse-grained models for RTILs to complement numerically intensive computer simulations. The strong correlations in RTILs pose a challenge to computer simulation methods, which are slow to converge in these stiffly coupled systems. Furthermore, the modelling of RTILs in non-uniform environments, such as fluids confined in pores, are made more difficult due to the requirement of chemical equilibrium.

The aim of the present work is two-fold. Firstly, we will incorporate ion pairing into the DFT. This theory provides an ideal framework to introduce the occurrence of clusters, as it relies upon free energy minimization of defined fluid densities in the presence of physically motivated constraints (such as the fraction of ion pairs). The formalism developed here can also be generalized to include larger neutral clusters, or specific clusters of say cation-cation pairs due to $\pi - \pi$ stacking in alkyl-imidazoliums. The coarse-grained RTIL model has been previously described [5, 28, 29]. Secondly, we will explore the implications of ion pair formation on a number of the predictions of the DFT. This is an interesting test, as the DFT *without* ion pairing proves to be very accurate when compared with the structural properties extracted from simulations on an identical coarse-grained model. Clearly, any modification of the theory, must take cognizance of that fact. While the debate about the degree of ion pair formation in RTILs remains open, it is of interest to determine the measurable consequences of imposing this type of constraint into our DFT approach. More specifically, we will explore the impact of ion pairing on the structure, capacitance and surface forces of an RTIL in the presence of electrodes.

II. MODELS AND THEORY

A. Coarse-grained model for ion pairing in RTIL

The oligomeric models for the *1-butyl-3-methyl imidazolium* cation $[C_4MIM^+]$ and the *tetrafluroborate* anion $[BF_4^-]$ are illustrated in Figure 1(a) and 1(b) respectively. Both species are made up of tangentially connected hard spheres with equal diameters $\sigma = 2.4$Å. The imidazolium ring on the cation is modelled as a star-like structure consisting of a central bead and four others attached peripherally. Each bead carries a partial charge of +0.2e. A similar star of 5 negative beads (each carrying -0.2e) is used to mimic the molecular structure of $[BF_4^-]$. The partial charges chosen here reflect an 'average" charge distribution. The electrostatic interaction between any two partial charges, q_α and q_λ, separated by r is given by,

$$\Phi_{el}^{\alpha\beta}(r) = \frac{1}{4\pi\epsilon_0\epsilon_r}\frac{q_\alpha q_\beta}{r} \tag{1}$$

where ϵ_0 is the permittivity of vacuum, and ϵ_r is due to the contributions to the low frequency dielectric response. These contributions arises from electronic and intra-molecular polarizability. We use, $\epsilon_r = 2.3$, which is typical for hydrocarbon groups. In addition to electrostatic and steric forces, all beads are also assumed to interact via the long-range attractive component of the Lennard-Jones potential at separations greater than σ.

$$\Phi_{att}(r) = -4\epsilon_{LJ}(\frac{\sigma}{r})^6 \tag{2}$$

The attractive strength is given by $\epsilon_{LJ}/k_B = 100K$ where k_B is Boltzmann's constant and $\sigma = 2.4$Å is the same as the hard sphere diameter of the beads. This model is identical to the one developed in recent molecular simulations.[30]

B. Polymer density functional theory

The DFT used for RTILs has been described previously in some detail [31–33]. In this theory, the free energy is expressed as a functional of the oligomeric densities for the RTIL model (as defined below). Equilibrium properties are obtained by minimizing the resulting free energy functional with respect to these densities. Here we will introduce a modification to this (now standard) DFT by including the possibility of ion pairing.

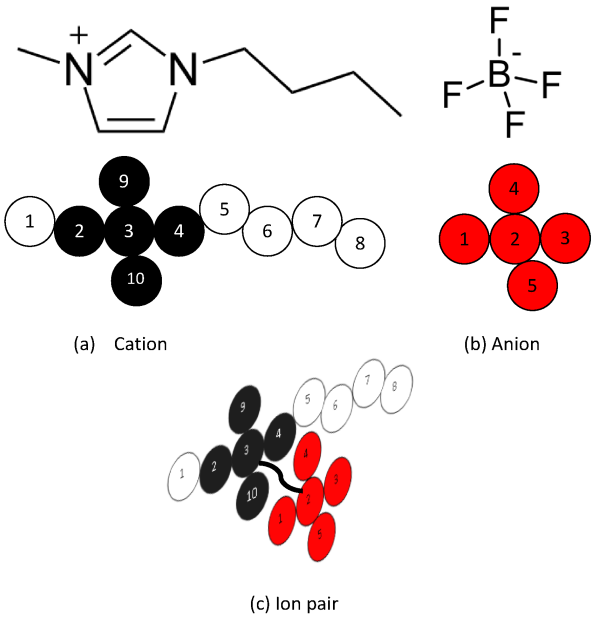

FIG. 1: Coarse-grained model of cations $[C_4MIM^+]$, anion $[BF_4^-]$ and neutral species ion pairs. Coloured spheres are charged whilst the rest are neutral.

We assume that ion pairing is an outcome of strong electrostatic interactions between oppositely charged ions although other sources of association, e.g., the stacking of cationic aromatic rings may also be present. That is, we make the intrinsic assumption that strong non-linear correlations responsible for ion association, are missing in the present version of the DFT. Ideally, the degree of ion pairing should be determined self-consistently through minimization of the free energy, which in many applications of DFT will be carried out on a fluid which is responding to an external field. There are certain thermodynamic factors which will determine the degree of ion pairing. For example, ion pairing or ionic clustering will in general lower the electrostatic energy of the system. However, the translational constraints of cluster formation will also have an accompanying entropic cost. Additionally, when a certain fraction of particles are constrained to form clusters, the local cluster density will usually be higher than the average fluid density. Thus there will be an overall increase in free volume of the fluid, leading to smaller steric contributions to the entropy. Both of these entropy contributions feature in the DFT treatment presented here, they derive from a similar treatment of equilibrium (or living) polymers [34].

Here, we will explore a simple realization of ion pair formation within a DFT framework,

whereby we will assume the existence of ion pairs (but no larger clusters) *a priori*. We propose to attribute this strong association to a (constant) correlation free energy between anions and cations as measured by the ion-pairing chemical potential in the bulk fluid, μ_p. The number of ion pairs is expected to depend upon local thermodynamic factors, which are accounted in our theory by minimizing the overall free energy with respect to the number of ion pairs in a nonuniform environment. The chemical potential, μ_p, accounts for contributions to ion-association, which are essentially independent of excess thermodynamic properties (beyond that of the bulk). Mathematically, it can be considered as a Lagrange multiplier, which *constrains* the fluid to display a certain fraction of ion pairs in the bulk. Free energy minimization in a non-uniform environment (at fixed μ_p) accounts for variations in this fraction as a response to applied fields.

An ion pair consists of an anion and a cation constrained to lie within a characteristic "pair distance", l_p, from one another. Specifically, a pair is created by joining the central bead in the positively charged star moiety in the cation to the central bead of the anion via an ideal and infinitely flexible "string" of length l_p, as shown in Figure 1(c). We note that, as the fraction of pairs is maintained to be in equilibrium with a bulk reservoir, this bonding potential serves only as a virtual constraint and pairing is implicitly reversible. The pair distance, l_p, is somewhat arbitrary, but would reasonably be expected to be slightly greater than σ. A series of string lengths were tested and only minor differences in the fluid properties were found. A value $l_p = 1.2\sigma$ was chosen in all the calculations reported below. The grand potential functional Ω used in this work will have the generic form,

$$\begin{aligned}\Omega \;=\; & F^{id}[N_c(\mathbf{R}), N_a(\mathbf{R}), N_p(\mathbf{R})] + F_{hs}[\bar{n}_s(r)] + F_{disp}[n_s(r))] + F_{corr}[n_c(r), n_a(r)] \\ & + F^{el}_{surf}[n_c(r), n_a(r)] + F^{disp}_{surf}[n_s(r)] - \sum_{\alpha}(\mu_\alpha + q_\alpha \Psi_D) \int d\mathbf{R} N_\alpha(\mathbf{R}) \end{aligned} \tag{3}$$

Here $\{N_\alpha(\mathbf{R}); \alpha = c, a, p\}$ is the set of oligomeric densities describing the cation, anion and paired species, respectively, where $\mathbf{R}$ is the coordinate vector representing the sites of the constituent beads. The quantities $\{n_\beta(\mathbf{r}); \beta = c, a, n, s\}$ describe the collected site densities of positive, negative and neutral beads, as well as their sum, respectively. They are obtained as integrals over the oligomeric densities,

$$n_\beta(r) = \int d\mathbf{R} \sum_\alpha \sum_i \delta(\mathbf{r} - \mathbf{r}_i) N_\alpha(\mathbf{R}) \tag{4}$$

where $\delta(\mathbf{r})$ is the Dirac delta function. The sum i runs over all beads of type β, in the

species α, where α selects from all 3 species types: cation, anion and ion-pairs. The total site density is given by, $n_s(\mathbf{r}) = n_c(\mathbf{r}) + n_a(\mathbf{r}) + n_n(\mathbf{r})$. In Eq.(3), μ_α is the chemical potential of species α in the bulk; q_α is the charge of species α and Ψ_D is the Donnan potential, which maintains electroneutrality. Equilibrium properties are obtained by minimizing the free energy with respect to the set of oligomeric densities, $\{N_\alpha(\mathbf{R}); \alpha = c, a, p\}$. We will briefly describe the explicit contributions to the free energy functional.

1. Ideal chain term

The ideal chain contribution to the free energy is given by:

$$\begin{aligned} F^{id}[N_c(\mathbf{R}), N_a(\mathbf{R}), N_p(\mathbf{R})] \; = \; & \sum_{\alpha=c,a,p} \int N_\alpha(\mathbf{R}) \left(\ln[N_\alpha(\mathbf{R})] - 1\right) d\mathbf{R} \\ & + \sum_{\alpha=c,a,p} \int N_\alpha(\mathbf{R}) (V_\alpha^{(B)}(\mathbf{R}) + V_\alpha^{ex}(\mathbf{R})) d\mathbf{R} \end{aligned} \tag{5}$$

where $V_\alpha^{(B)}(\mathbf{R})$ is the bonding energy and $V_\alpha^{ex}(\mathbf{R})$ is the external potential. For a straight chain segment of length N, the bonding potential is defined by,

$$e^{-\beta V_\alpha^{(B)}(\mathbf{R})} = \prod_{i=1}^{N} \delta(|\mathbf{r}_i - \mathbf{r}_{i+1}| - \sigma) \tag{6}$$

where $\delta(x)$ is the Dirac delta function and β is the inverse thermal energy. For the more complicated molecular topologies used in this work, a more complex connectivity applies. The ion pairing bond between the central bead of the cation $c3$ and the central bead of anion $a2$ (nomenclature is as illustrated in Figure 1) differs from the rigid bond within the cations and anions. It is given instead by

$$e^{-\beta V_{pair}^{(B)}(\mathbf{R})} = \Theta(l_p - |\mathbf{r}_{c3} - \mathbf{r}_{a2}|) \tag{7}$$

where the Heaviside function $\Theta(x)$ is defined as: $\Theta(x) = 1$ for $x > 0$ and $\Theta(x) = 0$ for $x \leq 0$.

2. Hard sphere term

The hard sphere contribution to the free energy, $F_{hs}[\bar{n}_s(r)]$, accounts for the entropy arising from the excluded volume interaction between all beads. We recall that all beads have the same hard sphere diameter. This is not a requisite of the theory, but merely

simplifies the algebra. A model, more finely tuned to specific RTILs would remove this simplification. To estimate this term, we will use the generalized van der Waals approach of Nordholm [35], which uses a single weighted density, i.e.,

$$\bar{n}_s(r) = \frac{3}{4\pi\sigma^3} \int_{|r-r'|<\sigma} n_s(r')dr'. \tag{8}$$

This has since been generalized to obtain a highly non-linear functional, $F_{hs}[\bar{n}_s(r)]$, of the weighted density, derived from the generalized Flory-Dimer equation of state [32, 36].

3. van der Waals interactions

The van der Waals interactions are modelled via the attractive part of the pairwise Lennard-Jones (L-J) potential, Eq.(2). Its contribution to the free energy takes a mean-field form, being an integral over $\Phi_{att}(r)$ with a short-range cut-off equal to the steric diameter, σ,

$$F_{disp}[n_s(r), n_s(r')] = \frac{1}{2} \int \int_{|r-r'|)\geq\sigma} n_s(r) n_s(r') \Phi_{att}(|r-r'|) dr \tag{9}$$

4. Electrostatic correlations

In dense RTILs, ions of like charge repel each other to create a"coulomb hole". This amounts to removing the self-term from the mean-field electrostatic energy. On the other hand, those of unlike charge are strongly correlated. These electrostatic correlations are critical for the description of overscreening by RTILs at charged electrodes. In previous work we introduced a very accurate, albeit approximate measure of the electrostatic correlations [30, 37]. In the present approach, we will include ion-pairs as a component of unlike ion correlation. The total cation and anion densities that appear in the electrostatic correlation term will have contributions from non-associated anions and cations as well as paired species. We take the point of view that the original functional only accounts for weak correlations, due to ions interacting with a surrounding atmosphere of countercharge. In our new theory, we assume that in addition to those weaker correlations, there is a non-linear correlation contribution leading to pair formation.

The specific form of the electrostatic correlation functional, F_{corr} is usefully split into

separate contributions, F_{corr}^{like} and F_{corr}^{unlike}, where,

$$F_{corr}^{like} = \frac{1}{2}\int\int \sum_{\alpha=a,c} n_\alpha(r) n_\alpha(r')(1 - e^{-\lambda|r-r'|})\Phi_{el}^{\alpha\alpha}(|r-r'|)drdr' \tag{10}$$

$n_\alpha(r)$ denotes the density of charged beads, including contributions from both separate and paired species; Φ_{el} is coulomb interaction defined earlier, (Eq.1). The parameter λ is determined by electroneutrality in the bulk (as the correlation hole represents the removal of the self contribution from the background) [30, 38]. Unlike ion correlations are approximated with the functional,

$$F_{corr}^{unlike} = \frac{1}{2}\int\int \sum_{\alpha\neq\beta} n_\alpha(r) n_\beta(r')\Theta(|r-r'| - d_{\alpha\beta})\Phi_{el}^{\alpha\beta}(|r-r'|)drdr' \tag{11}$$

where the radius of the "hard coulomb hole" is given by $d_{\alpha\beta} = \chi\sigma$. The parameter χ is chosen to fit the simulated bulk density of the same model, under ambient pressure and temperature [30]. For the RTIL $[C_4MIM^+][BF_4^-]$, described above, the conditions used in this work are a temperature of 298K and pressure of $1atm$. Thus the new theory is adjusted for the presence of ion pairs in a consistent way.

5. Surface-fluid interaction

The interactions between the surface and fluid give rise to a coulombic contribution, F_{surf}^{el}, and a dispersion contribution, F_{surf}^{disp}. F_{surf}^{el} accounts for all electrostatic interactions between the surface and the RTIL particles. We assume that the surface charges are smeared out, thus defining a uniform surface charge density. The dispersion interaction is evaluated by integrating the 12-6 Lennard-Jones potential over both planar half-spaces. For a single half-space, that integral is given by

$$\omega_{LJ}(z) = 2\pi\epsilon_{LJ}\left[\frac{2}{45}(\frac{\sigma_w^9}{z^9}) - \frac{1}{3}(\frac{\sigma_w^3}{z^3})\right] \tag{12}$$

where z is the distance from the surface plane to the bead center. The L-J term from the other surface is obtained by replacing z with $(h-z)$, where h is the surface separation. The L-J parameters are the same as for the bead-bead interactions. [30]

The equilibrium density profiles are obtained by minimizing the total free energy (Eq.3), with respect to the oligomeric cation and anion densities as well as the ion-pair density, at fixed chemical potentials for all species. We note that, for finite separations between the

surfaces, the Donnan potential must be solved self-consistently in order to obtain electroneutrality.

III. RESULTS AND DISCUSSION

A. Spatial distribution profiles

We considered two oppositely charged surfaces separated by 20σ, with left surface negatively charged (inverse surface charge density of -320Å$^2/e$) and the right surface positively charged (+320Å$^2/e$). The density distributions for single cations and anions are plotted (Fig.2) at 0% pairing in the bulk. A typical feature of RTILs at electrified interfaces are the

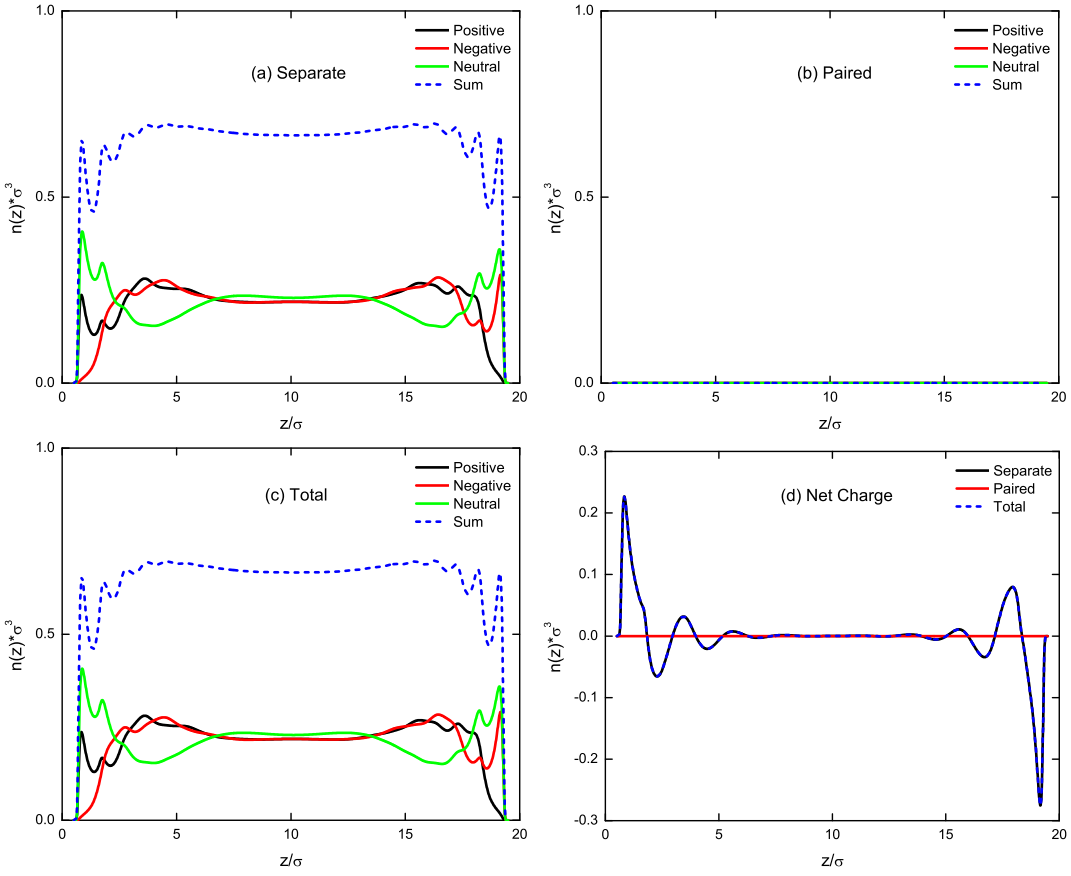

FIG. 2: At 0% pairing. Electrode surfaces are of equal and opposite charge density (320Å$^2/e$). We plot denity profiles for positive, negative, neutral beads as well as the sum of beads for (a) separate species (b) paired species (c) total of the two; and (d) net charge profiles.

alternating layers of counter-ion and co-ions, observed adjacent to both surfaces. Overscreening occurs as the first layer delivers more counter-ion charge than surface charge. There is a noticeable asymmetry in the system, due to the differences between the intramolecular structure of the anions and cations. We find that screening is stronger at the positive electrode, as the anions are able to approach the surfaces more easily than cations. As cations are larger oligomers there is a greater loss in configurational entropy as they approch the surface compared to anions.

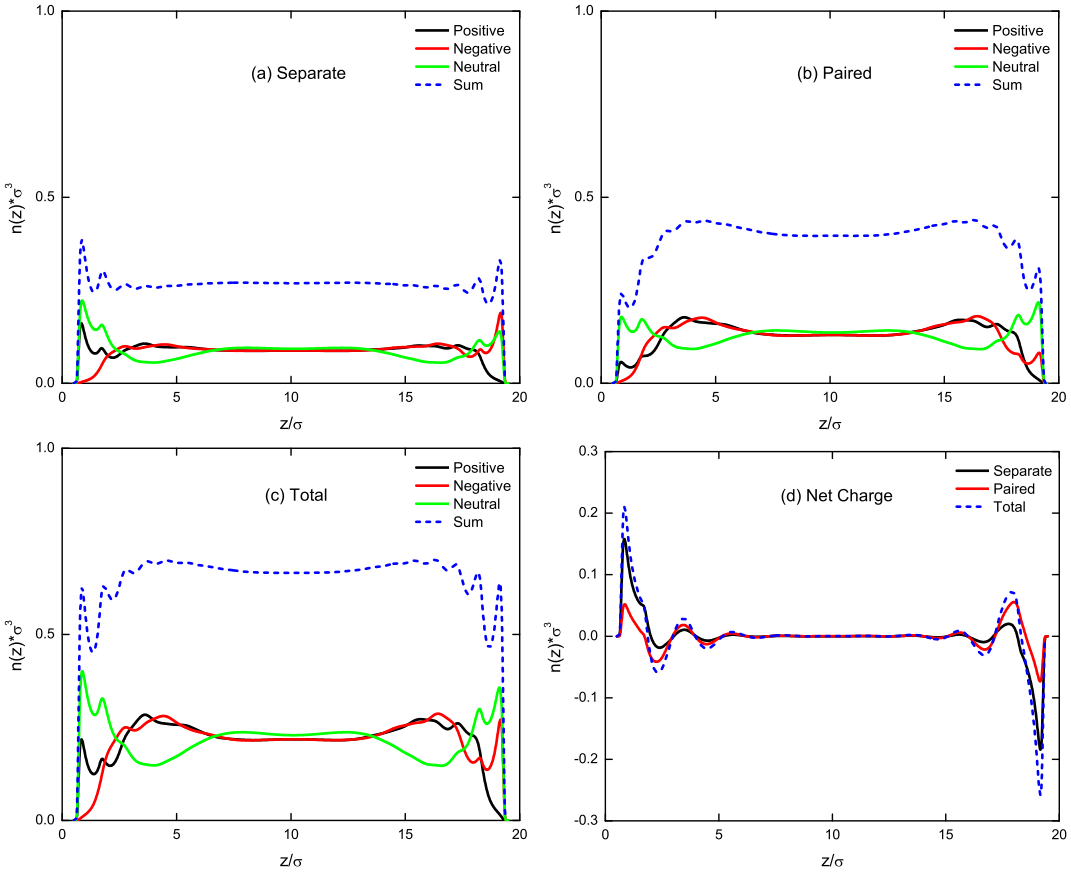

FIG. 3: At 60% pairing. Electrode surfaces are of equal and opposite charge density ($320\text{Å}^2/e$). We plot denity profiles for positive, negative, neutral beads as well as the sum of beads for (a) separate species (b) paired species (c) total of the two; and (d) net charge profiles.

Figure 3 shows the results of increasing the fraction of pairs to 60% in the bulk. This degree of ion pairing is suggested by experimental measurement of conductivity and diffusion [25]. Despite having a larger concentration in the bulk than dissociated ions, ion pairs only makes up for approximately one third of the counter charge in the counterion peak adjacent

to the surfaces. This is clearly seen in the contributions to the net charge profiles in Fig 3(d). Separate species are responsible for a reasonably larger proportion of the screening. Based on the location of counter-ions and co-ions peaks, ion pairs tend to orient themselves perpendicularly to the charged surfaces. Similar observations of ion pairs aligning perpendicularly to the surface are made in experiments of RTILs [8]. A comparison of Figure 2 and 3, show a hardly discernable difference in the total ion density profiles despite the different amount of ion paring. The relative low number of ion pairs close to the surfaces is due to the configurational entropy penalty, as well as electrostatic repulsion of the co-ion partner. Ion pairs are effectively large oligomeric structures and suffer a greater configurational entropy loss compared to single species. Furthermore, they are dipoles and hence are less effective at screening the electrode charge compared with single species.

Recent surface force measurements by Gebbie *et al* indicate that ion association may dominate the equilibrium structure of RTILs [11]. Those authors suggest that the degree of association may be as high as 99.997%, which is a significant paradigm shift in the way RTILs are viewed. Surprisingly, when we increased the degree of ion paring to this value, we found only very minor changes in the total density profiles. In this case, the major part of the screening is carried out by the paired species, but the total charge density profile is very similar to systems with no ion paring. Thus ion pairs now play the major role in establishing these very similar charge density profiles.

It is interesting to study the system where the fraction of ion pairing is 100%. In this case, the fluid consists of dipolar molecules and is unable to screen surfaces with a net charge. However, the fluid between oppositely charged surfaces should behave as a dielectric medium. Despite the complete pairing, the ionic density profiles again show very similar features to those with fractional pairing, as displayed in Figure5 (a)-(d). Apparent overscreening of the electrodes persist, when only ion pairs are present. To rationalize this phenomenon, we present a schematic figure to show how a system with 100% pairing (Fig.6(a)) can give rise to exactly the same average density profile (same number of charges per layer) as a more dissociated ionic liquid (Fig.6(b)).

By integrating the net charge density in Figure 5 (d), from the surface plane to the mid-plane, we find that the surface charge of both surfaces are screened by 95.7%, indicating a strong but incomplete screening of electrode. This should give rise to a weak electrostatic attraction between the oppositely charged surfaces. Its energy contribution will be linear

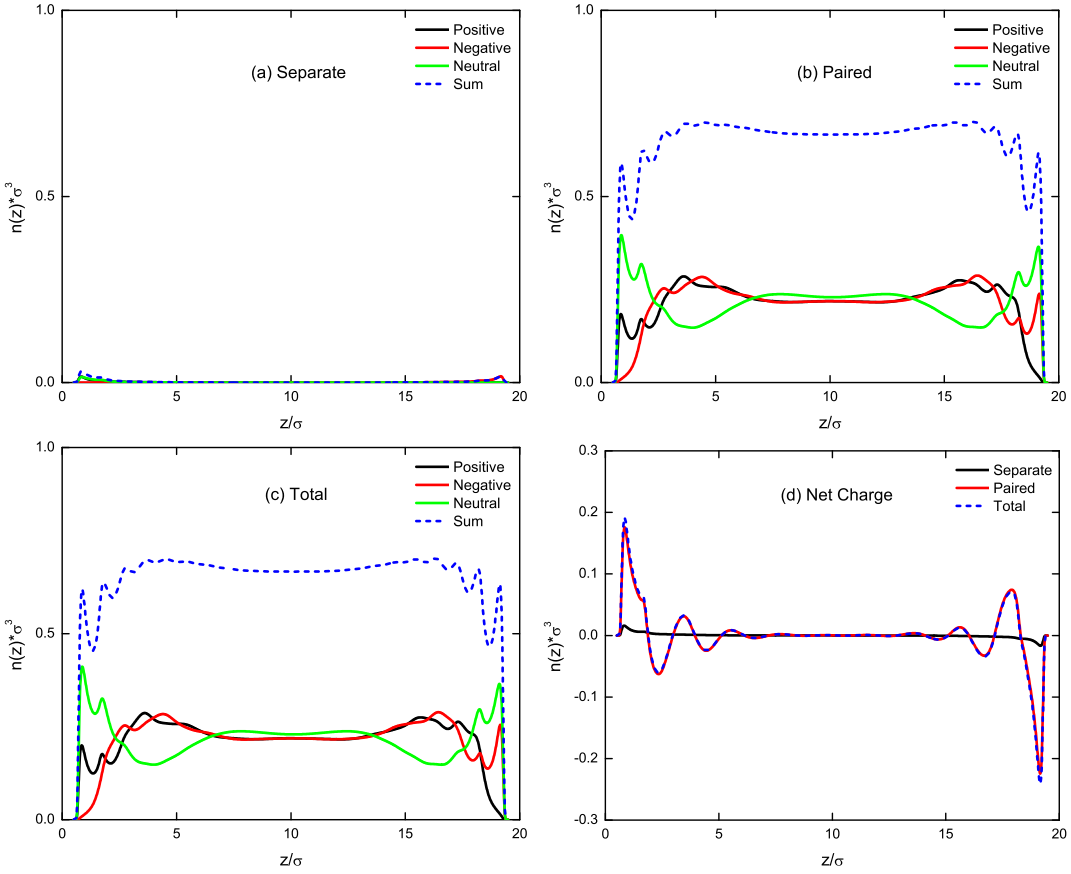

FIG. 4: At 99.997% pairing. Electrode surfaces are of equal and opposite charge density (320Å$^2/e$). We plot denity profiles for positive, negative, neutral beads as well as the sum of beads for (a) separate species (b) paired species (c) total of the two; and (d) net charge profiles.

with the separation, h. This attractive force is confirmed in the later discussion of surface forces.

Finally, we report the results for the case of two surfaces with similar surface charge density of -320Å$^2/e$, with the degree of bulk ion-pairing set at 99.9%. Figure 7 displays the spatial distribution profiles. The profiles are symmetric as the two surfaces are indistinguishable. At this large degree of ion-paring, the charged density profile and, in particular the overscreening of the electrodes, is dominated by the orientation of ion pairs. Long-range screening by dissociated species (Fig.7(d))is detectable for the neutralization of the charges on both surfaces. As the ion-pairs contribute no charge, this long-range screening reflects the large Debye length in an effectively a dilute electrolyte, as suggested in the surface force measurements by Gebbie *et al.* [11].

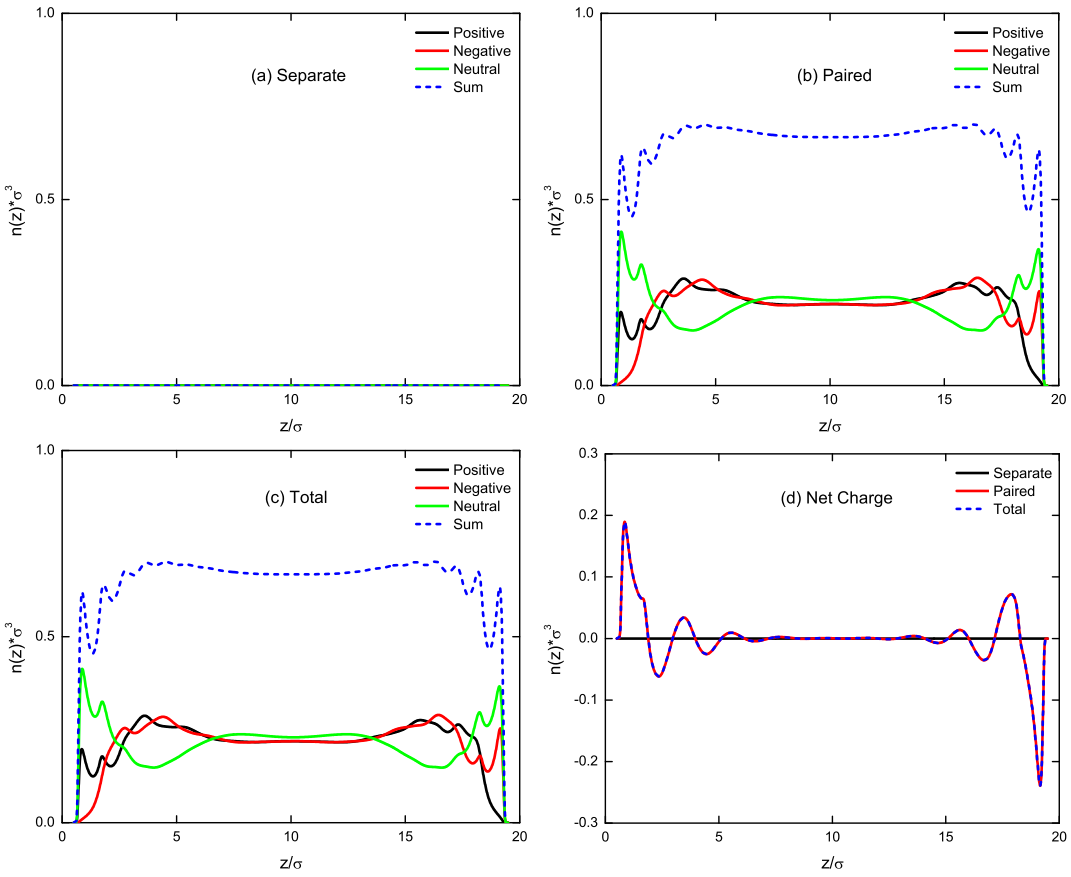

FIG. 5: At 100% pairing. Electrode surfaces are of equal and opposite charge density (320Å$^2/e$). We plot denity profiles for positive, negative, neutral beads as well as the sum of beads for (a) separate species (b) paired species (c) total of the two; and (d) net charge profiles.

B. Comparison with simulations: short-range structure

According to the results above, the incorporation of even complete ion pairing into the DFT does not significantly change the density profiles of positive, negative, neutral and total beads (sum of all species). This is further demonstrated in Figure 8 where we compare the total density as well as the net charge density profile against a single negative surface (-320Å$^2/e$).

The influence of ion pairing on these density profiles is very small and, more importantly, the agreement with simulations remains, especially for the net charge density. It is somewhat reassuring that the inclusion of ion pairs does not compromise that agreement in the extended theory. This result suggests that short-range structural information gathered at

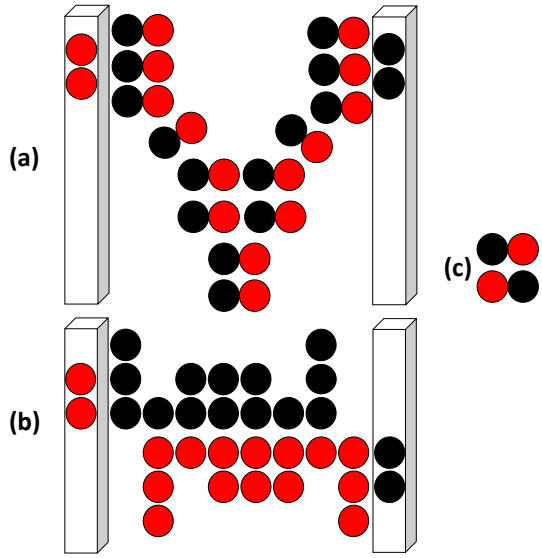

FIG. 6: Between oppositely charged double surfaces (a) schematic representation of overscreening by non-uniformly compressed ion pairs (b) equivalent distribution by free ions (c) dipoles compensate each other to build bulk-like profiles

the electrified interface does not provide a conclusive test as to whether significant ion pairing is a real phenomenon in RTILs. In this context, we note that only small differences in density and charge profiles are also observed for various degrees of ion pairing near more weakly charged electrodes. Instead, as we shall see below, the effect of ion pairing asserts itself in the long-range *tails* of these structures. These long-range effects are exhibited in the decay of the electrical potential as well as asymptotic surface forces.

C. Forces between charged surfaces

From the equilibrium density profiles we are also able to evaluate the surface forces acting on the surfaces. Figure 9 summarizes the equilibrium pressures (force/area) on oppositely charged surfaces with absolute inverse surface charge densities of $320\text{Å}^2/e$. In the absence of ion-paring we see a relatively short-range pressure profile with oscillations, due to the sequential removal of ionic particle layers from between the surfaces. as the latter are brought together. As the system must keep electroneutral, pairs of ions must be removed together, which explains why oscillations have a spacing roughly equal to the diameter of an ion pair, around 10σ. At longer range the attraction decays rapidly.

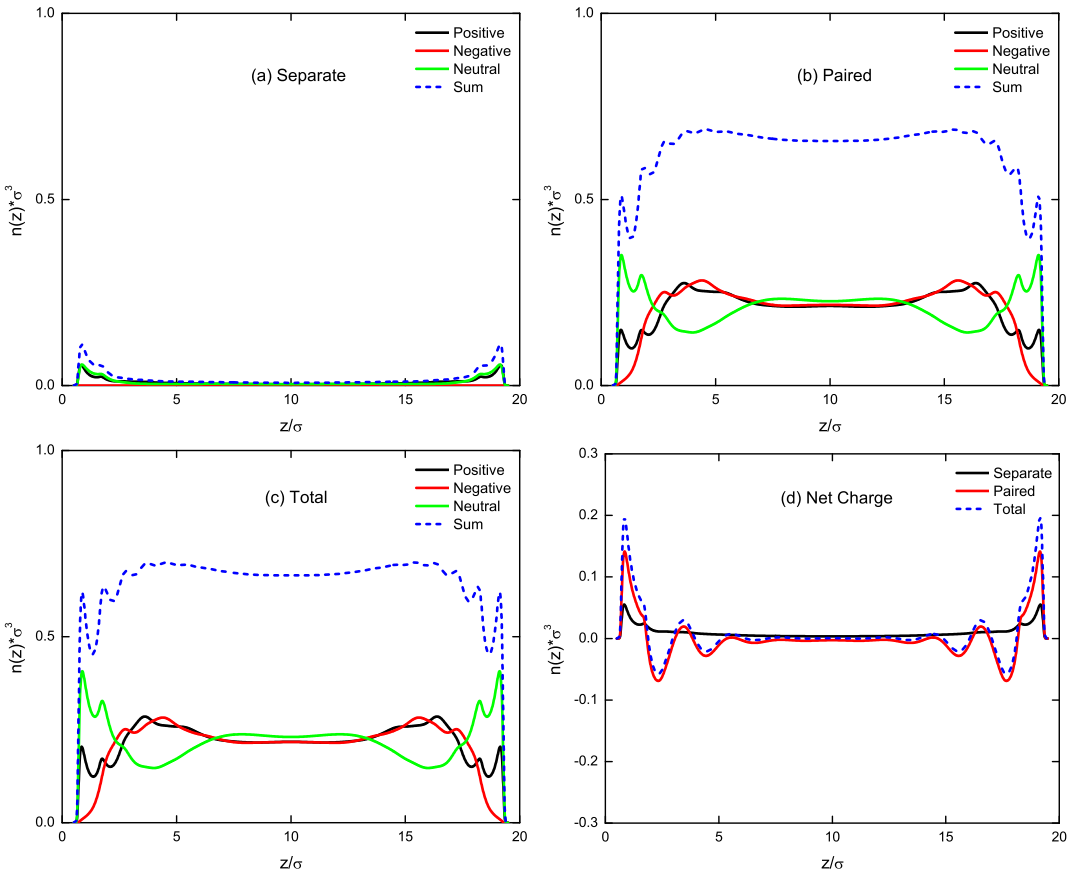

FIG. 7: At 99.9% pairing, between double negaive surfaces of -320Å$^2/e$, density profiles of positive, negative, neutral beads as well as the sum of beads for (a) separate species (b) paired species (c) total of the two; and (d) net charge profiles.

As the degree of ion paring increases, the first peak in the pressure profile remains somewhat invariant. At these short separations ($h \approx 5\sigma$), there is a high density layer of positive and negative ions oriented perpendicular to the surfaces, regardless the concentration of ion pairs. This high internal density of particles generates a strong repulsive pressure. As the distance increases, ($h \approx 10\sigma$) the overall density of species decreases because the double surfaces are not sufficiently separated to allow the influx of a substantial number of particles. This leads to an attractive trough as the pressure in the slit becomes less than the bulk value. This effect is more pronounced for ion pairs, which suffer a greater depletion interaction with the surfaces compared with dissociated species.

At large separation, a long-range attractive tail is observed. This tail becomes more obvious as the degree of ion paring grows. By analogy with double surfaces immersed in dilute

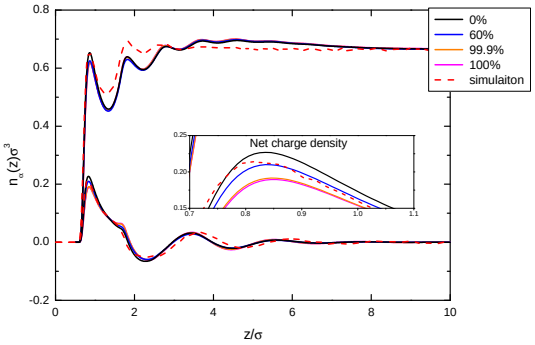

FIG. 8: Comparing total bead densities (upper group of curves) and net charge densities (lower group of curves) from DFT treatment across all degrees of ion pairing. Inset shows the minor distinction in the first peak of net charge density curves brought by variation of pairing degree.

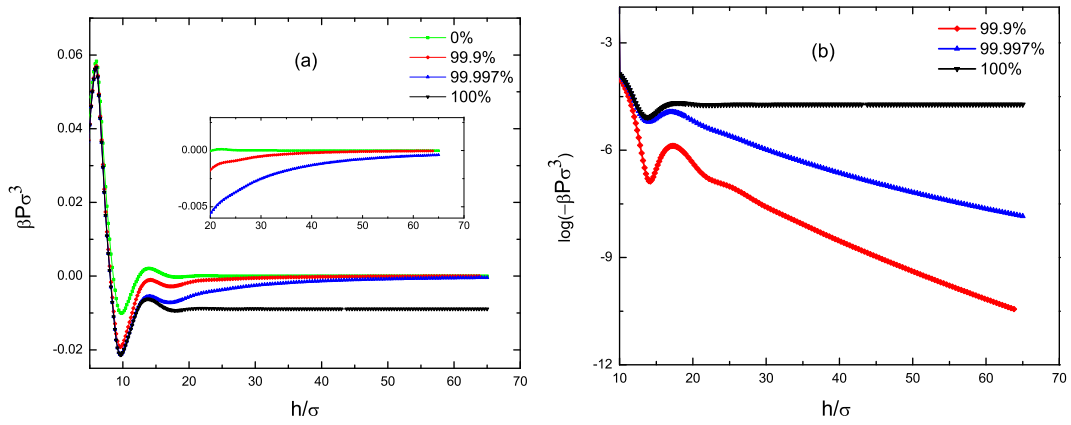

FIG. 9: (a) surface forces as a function of separation between oppositely charged double surfaces at different degrees of pairing (b) logarithm of minus surface force as a function of separation

electrolytes, we expect that this long-range tail would have an exponential form, with decay length equal to the Debye length appropriate to the concentration of the dissociated ions. In Figure 9(b), the logarithm of the absolute surface pressure is plotted. Linear behaviour is found, particularly for separations larger than 20σ, which confirms an exponential decay. We also note that the slope of decay is greater at lower pairing fraction, in line with a shorter Debye length expected. For 100% pairing, the tail becomes flat as evidenced by a constant negative pressure.

Next we consider forces between two negatively charged surfaces in Figure 10. Both surfaces have a negative charge density corresponding to a surface area per charge of $320\text{Å}^2/e$.

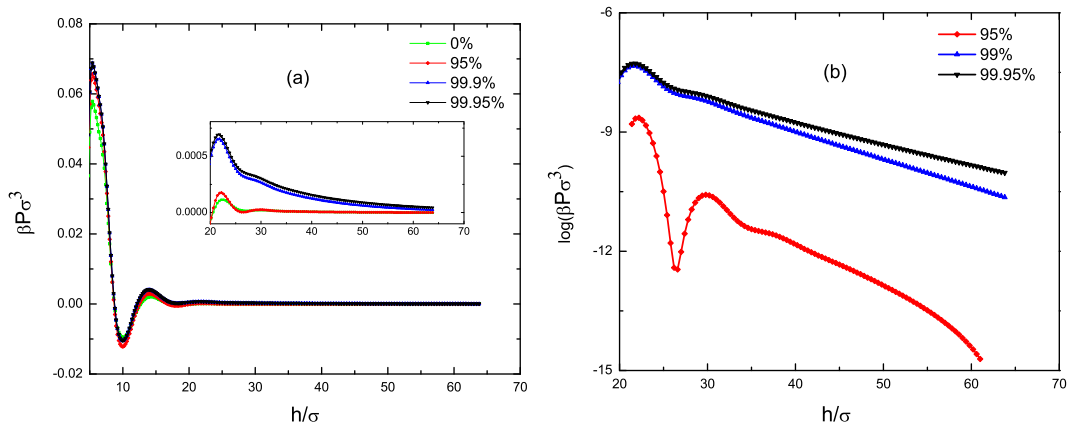

FIG. 10: (a) surface forces as a function of separation between similarly charged double surfaces at different degrees of pairing (b) logarithm of surface force as a function of separation

Unlike the case of oppositely charged surfaces, the first peak of the pressure between like charged surfaces is larger in those systems with higher ion pairing. This is because the ion pairs are not able to contribute net charge into the slit. The additional counterions required to neutralize the surfaces causes the overall internal particle density to increase with a correspondingly larger repulsive pressure.

A long range component is noticeable as well in the surface pressure, which is repulsive, due to the same sign of the surface charges. However, this long-range repulsion is not significant until the degree of ion pairing becomes exceptionally large. Even at 95% ion pairing, the repulsion appears weak, see inset in Figure 10(a). At an ion pairing fraction of 99.95% and higher, there is a larger repulsion displayed by the asymptotic region of the pressure curves, see inset in Figure 10(a). This is probably due to the poorer screening of charge in these systems. As with the unlike charged surfaces, we see in Figure 10(b), that the decay length of the force curve decreases with less ion pairing. Our pressure profiles predict short-range oscillations and long-range Debye-Huckel decay at high degree of ion pairing, consistent with SFA measurements of Gebbie *et al*,[11].

So, as preempted in our earlier discussion, ion pairing has a more significant effect on the asymptotic behaviour of surface forces. This is due to the long-range decay of the potential profile arising from a large effective Debye length. These effects are probably difficult to observe in simulations, due to the size of the system that would be required, as well as the small magnitude of the net pressures involved.

D. Differential capacitance

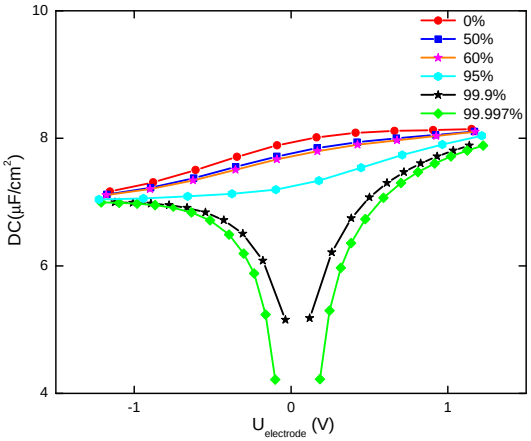

FIG. 11: DC of $[C_4MIM^+][BF_4^-]$ model as a function of surface potential at different degree of pairing

Ion pairing has been attributed a role in the unusual temperature dependence of the capacitance of EDLC [6, 14, 24]. It is of interest to investigate the impact of ion paring on the differential capacitance (DC) of a capacitor employing an RTIL. The DC per unit area is computed as numerical derivative of the surface charge density with respect to the surface electrical potential. In our calculations, the surface charge density ranges from $-0.10C/m^2$ to $+0.10C/m^2$. Figure 11 compares the DC curves as a function of electrode potential at different degrees of ion pairing. Across all degrees of ion pairing, the DC tends to be higher at a positive electrode potential compared to a negative one. The larger DC at the positive electrode is generally attributed to the greater ability of the smaller anion to screen surface charges [38]. However, a monotonic decrease is observed for the DC in general, across a wide potential range, with increasing amounts of ion pairing (Fig.11). This is because fewer free ions are available to efficiently screen the electrodes as the pairing fraction increases. This effect is quite significant at around zero potential, where a minimum in the DC appears. The DC displays the so-called "camel-shape" at the two highest degrees of ion pairing considered in this study. The prevalence of ion pairing in these latter systems leads to more diffuse double layers of dissociated ions at low potential. As the surface potential increases, the dissociated ions respond non-linearly to provide greater screening. Thus, in this model, the DC vs surface potential curve transforms from bell to camel shape as the degree of ion pairing increases. More ion pairing implies that the overall cohesive energy of the RTIL

is increasing. Hence, this mechanism is similar to one articulated in simulation studies by Trulsson et al [39], who considered the effect of cohesive energy on the DC brought by dispersion forces within the RTIL. Noting that a higher temperature is expected to reduce the degree of ion pairing, our results support the suggestion that ion association may be responsible for the positive temperature dependence of the DC [9, 24]. Furthermore, we also observe that the effect of ion pairing on the DC becomes less pronounced at larger electrode potentials (Fig.11). This is consistent with the smaller influence of temperature on the DC at larger surface potential, as is seen in experiments and simulations [9, 20]. However, it is also important to note that increasing temperature will tend to cause the EDL to become more diffuse, which will, to some extent, counter the effect of increasing the availability of free ions.

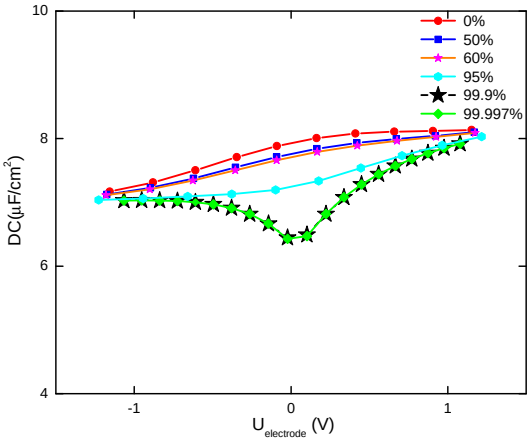

FIG. 12: At $d_{cut}/\sigma = 10$, DC as a function of surface potential at various degree of pairing

The small differences in short-range structure suggest that it is the tail part of the charge density that is primarily responsible for the minimum (and hence the camel shape) in the DC profile at high degree of pairing. To assess this, we recalculated the DC profiles by defining the surface potential relative to the potential at a certain cut-off distance, d_{cut}, from the surface, rather than the bulk. The latter would correspond to $d_{cut} \to \infty$. The resulting DC profiles for various degrees of ion pairing are plotted for $d_{cut}/\sigma = 10$ (Fig.12). We see that at extremely high degree of pairing, the DC profiles deviate from the results without the cut-off (Fig.11). In the DC profiles obtained at 99.9% and 99.997% pairing, the minima are significantly diminished. This effect is further exemplified in Fig.13, which compares the DC profiles obtained for the cut-off distances $d_{cut}/\sigma = 5$ and 10 in the cases

of strong pairing. Clearly, the range of electric potential decay plays an important role in establishing the camel-shaped capacitance for the highly paired systems.

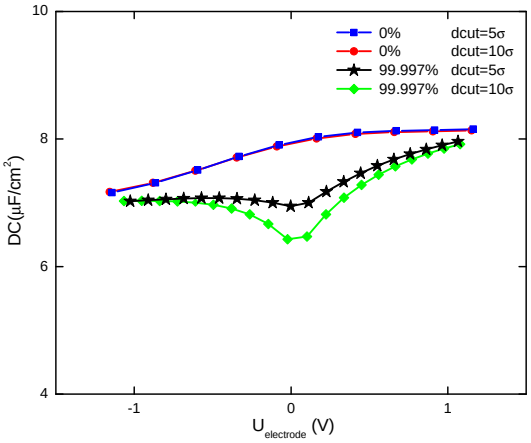

FIG. 13: Comparison of DC curves in cases of $d_{cut}/\sigma = 5$ and 10, for 0% and 99.997% degree of pairing

IV. CONCLUSIONS

We describe ion pairing in a coarse-grained model of aromatic RTILs within the theoretical framework of a classical DFT. Pairing is treated as a short-range, non-linear component of anion-cation correlations, complementary to the long-range correlations, also included within the free energy functional. The presence of ion pairs do not significantly affect the short-range structure at charged surfaces and good agreement with predictions from simulations is maintained irrespective of the degree of ion pairing. This implies that evidence for ion pairing may not be found in the short-range structures typically generated in simulations. Instead, ion pairing will only become apparent in properties which involve the long-range screening of charges. In our studies, this long-range effect is shown in the asymptotic behaviour of surface forces and the differential capacitance around low surface potentials. Both of these properties would hence be difficult to obtain accurately from simulations because of the system sizes required.

Ion paring and, indeed, ionic clusters in general (so-called Bjerrum clusters) have also been implicated in the anomalous temperature behaviour of the differential capacitance. The DFT predicts that ion pairing reduces the differential capacitance, particularly at low

electrode potential. Therefore, the temperature effect on the ion pair population remains a plausible explanation for the increase in capacitance at higher temperature.

Finally we note that any attempt to reconcile dynamic and equilibrium manifestations of ion pair formation would need to relate the free energy cost of equilibrium fluctuations with their rate of decay, as suggested by the *fluctuation dissipation theorem*. A dynamic version of our classical DFT provides a possible route to this, allowing for the rates of association and dissociation of ion pairs.

---

[1] Jason P. Hallett and Tom Welton. Room-temperature ionic liquids: Solvents for synthesis and catalysis. 2. *Chem Rev*, 111(5):3508–3576, 2011.

[2] Robin D. Rogers, Kenneth R. Seddon, American Chemical Society. Division of Industrial, Engineering Chemistry., and American Chemical Society. Meeting. *Ionic liquids : industrial applications for green chemistry*. American Chemical Society, 2002.

[3] Natalia V. Plechkova and Kenneth R. Seddon. Applications of ionic liquids in the chemical industry. *Chemical Society Reviews*, 37(1):123–150, 2008.

[4] H. Weingartner. Understanding ionic liquids at the molecular level: facts, problems, and controversies. *Angewandte Chemie*, 47(4):654–670, 2008.

[5] J. Forsman, C. E. Woodward, and M. Trulsson. A classical density functional theory of ionic liquids. *J Phys Chem B*, 115(16):4606–4612, 2011.

[6] Maxim V. Fedorov and Alexei A. Kornyshev. Ionic liquids at electrified interfaces. *Chem Rev*, 114(5):2978–3036, 2014.

[7] I. Krossing, J. M. Slattery, C. Daguenet, P. J. Dyson, A. Oleinikova, and H. Weingartner. Why are ionic liquids liquid? a simple explanation based on lattice and solvation energies. *J Am Chem Soc*, 128(41):13427–13434, 2006.

[8] Susan Perkin. Ionic liquids in confined geometries. *Phys Chem Chem Phys*, 14(15):5052–5062, 2012.

[9] Muhammad Tanzirul Alam, Jahangir Masud, Md Mominul Islam, Takeyoshi Okajima, and Takeo Ohsaka. Differential capacitance at au(111) in 1-alkyl-3-methylimidazolium tetrafluoroborate based room-temperature ionic liquids. *The Journal of Physical Chemistry C*, 115 (40):19797–19804, 2011.

[10] Niels Janniksen Bjerrum. *Untersuchungen ber Ionenassoziation.* Hst, 1926.

[11] M. A. Gebbie, M. Valtiner, X. Banquy, E. T. Fox, W. A. Henderson, and J. N. Israelachvili. Ionic liquids behave as dilute electrolyte solutions. *P Natl Acad Sci USA*, 110(24):9674–9679, 2013.

[12] Yu. V. Kalyuzhnyi, M. F. Holovko, and A. D. J. Haymet. Integral equation theory for associating liquids: Weakly associating 22 electrolytes. *The Journal of Chemical Physics*, 95(12): 9151–9164, 1991.

[13] Marcel Druschler, Natalia Borisenko, Jens Wallauer, Christian Winter, Benedikt Huber, Frank Endres, and Bernhard Roling. New insights into the interface between a single-crystalline metal electrode and an extremely pure ionic liquid: slow interfacial processes and the influence of temperature on interfacial dynamics. *Phys Chem Chem Phys*, 14(15):5090–5099, 2012.

[14] V. Lockett, M. Horne, R. Sedev, T. Rodopoulos, and J. Ralston. Differential capacitance of the double layer at the electrode/ionic liquids interface. *Phys Chem Chem Phys*, 12(39): 12499–12512, 2010.

[15] R. Costa, C. M. Pereira, and F. Silva. Double layer in room temperature ionic liquids: influence of temperature and ionic size on the differential capacitance and electrocapillary curves. *Phys Chem Chem Phys*, 12(36):11125–11132, 2010.

[16] Muhammad Tanzirul Alam, Md Mominul Islam, Takeyoshi Okajima, and Takeo Ohsaka. Capacitance measurements in a series of room-temperature ionic liquids at glassy carbon and gold electrode interfaces. *The Journal of Physical Chemistry C*, 112(42):16600–16608, 2008.

[17] Fernando Silva, Cristiana Gomes, Marta Figueiredo, Renata Costa, Ana Martins, and Carlos M. Pereira. The electrical double layer at the [bmim][pf6] ionic liquid/electrode interface effect of temperature on the differential capacitance. *J Electroanal Chem*, 622(2):153–160, 2008.

[18] V. Lockett, R. Sedev, J. Ralston, M. Horne, and T. Rodopoulos. Differential capacitance of the electrical double layer in imidazolium-based ionic liquids: Influence of potential, cation size, and temperature. *J Phys Chem C*, 112(19):7486–7495, 2008.

[19] Liis Siinor, Rauno Arendi, Karmen Lust, and Enn Lust. Influence of temperature on the electrochemical characteristics of bi(111)—ionic liquid interface. *J Electroanal Chem*, 689: 51–56, 2013.

[20] J. Vatamanu, L. Xing, W. Li, and D. Bedrov. Influence of temperature on the capacitance of

ionic liquid electrolytes on charged surfaces. *Phys Chem Chem Phys*, 16(11):5174–5182, 2014.

[21] X. Liu, Y. Han, and T. Yan. Temperature effects on the capacitance of an imidazolium-based ionic liquid on a graphite electrode: A molecular dynamics simulation. *Chemphyschem*, 15 (12):2503–2509, 2014.

[22] Dezso Boda, Kwong-Yu Chan, and Douglas Henderson. Monte carlo simulation of an ion-dipole mixture as a model of an electrical double layer. *The Journal of Chemical Physics*, 109 (17):7362, 1998.

[23] Dezso Boda, Douglas Henderson, and Kwong-Yu Chan. Monte carlo study of the capacitance of the double layer in a model molten salt. *The Journal of Chemical Physics*, 110(11):5346, 1999.

[24] Myroslav Holovko, Vitalyj Kapko, Douglas Henderson, and Dezs Boda. On the influence of ionic association on the capacitance of an electrical double layer. *Chem Phys Lett*, 341(34): 363–368, 2001.

[25] Hiroyuki Tokuda, Seiji Tsuzuki, Md Abu Bin Hasan Susan, Kikuko Hayamizu, and Masayoshi Watanabe. How ionic are room-temperature ionic liquids? an indicator of the physicochemical properties. *The Journal of Physical Chemistry B*, 110(39):19593–19600, 2006.

[26] Kenneth R. Harris, Mitsuhiro Kanakubo, Noriaki Tsuchihashi, Kazuyasu Ibuki, and Masakatsu Ueno. Effect of pressure on the transport properties of ionic liquids: 1-alkyl-3-methylimidazolium salts. *The Journal of Physical Chemistry B*, 112(32):9830–9840, 2008.

[27] Kenneth R. Harris and Mitsuhiro Kanakubo. High pressure studies of the transport properties of ionic liquids. *Faraday Discuss*, 154(0):425–438, 2012.

[28] Clifford E. Woodward. A density functional theory for polymers: Application to hard chain-hard sphere mixtures in slitlike pores. *The Journal of Chemical Physics*, 94(4):3183, 1991.

[29] R. Szparaga, C. E. Woodward, and J. Forsman. Theoretical prediction of the capacitance of ionic liquid films. *J Phys Chem C*, 116(30):15946–15951, 2012.

[30] M. Turesson, R. Szparaga, K. Ma, C. E. Woodward, and J. Forsman. Classical density functional theory & simulations on a coarse-grained model of aromatic ionic liquids. *Soft Matter*, 10(18):3229–3237, 2014.

[31] J. Forsman, R. Szparaga, S. Nordholm, C. E. Woodward, and R. Penfold. *Ionic Liquids - Classes and Properties*. InTech, Rijeka, 2011.

[32] J. Forsman and C. E. Woodward. Evaluating the accuracy of a density functional theory of

polymer solutions with additive hard sphere diameters. *J Chem Phys*, 120(1):506–510, 2004.

[33] Z. Li, D. Cao, and J. Wu. Density-functional theory and monte carlo simulation for the surface structure and correlation functions of freely jointed lennard-jones polymeric fluids. *J Chem Phys*, 122(17):174708, 2005.

[34] Clifford Woodward and Jan Forsman. Density-functional theory for polymer fluids with molecular weight polydispersity. *Phys Rev Lett*, 100(9), 2008.

[35] S. Nordholm, M. Johnson, and B. C. Freasier. Generalized vanderwaals theory .3. the prediction of hard-sphere structure. *Aust J Chem*, 33(10):2139–2150, 1980.

[36] C. E. Woodward and A. Yethiraj. Density-functional theory for inhomogeneous polymer-solutions. *J Chem Phys*, 100(4):3181–3186, 1994.

[37] J. Forsman and S. Nordholm. Polyelectrolyte mediated interactions in colloidal dispersions: hierarchical screening, simulations, and a new classical density functional theory. *Langmuir*, 28(9):4069–4079, 2012.

[38] Ke Ma, Clifford E. Woodward, and Jan Forsman. Classical density functional study on interfacial structure and differential capacitance of ionic liquids near charged surfaces. *The Journal of Physical Chemistry C*, 118(29):15825–15834, 2014.

[39] M. Trulsson, J. Algotsson, J. Forsman, and C. E. Woodward. Differential capacitance of room temperature ionic liquids: The role of dispersion forces. *J Phys Chem Lett*, 1(8):1191–1195, 2010.